# An Analytical and Experimental Investigation of Swirling Flow in Nozzles

DAVID J. NORTON,* B. W. FARQUHAR,† AND JOE D. HOFFMAN‡
*Purdue University, Lafayette, Ind.*

**This investigation consisted of an analytical and experimental study of swirling flow in converging passages. The governing equations for the rotating, inviscid, adiabatic, compressible flow of a perfect gas were derived and reduced to a set of two nonlinear, ordinary differential equations which were solved numerically. A correction for the effects of viscous dissipation was developed. The analytical results indicated that spin effects are reduced by decreasing the nozzle contraction ratio, propellant molecular weight, and burning rate exponent, and by increasing the flame temperature and specific heat ratio. An experimental cold-flow study employing air in a rotating motor was conducted. Studies were conducted to determine the effect of the vortex-nozzle interaction, termed vortex choking, on the mass flow rate through choked nozzles. The experimental results indicated that vortex choking is influenced by the type of vortex initially generated in the chamber, the nozzle contraction ratio, and the vortex strength. The chamber pressure, nozzle configuration, and location of the vortex generating surface in the chamber had little effect. The experimental results were compared to analytical predictions and were in good agreement with the viscous theory, indicating that the present analytical model appears to reasonably predict the effects of vortex choking.**

## Nomenclature

$A_t$ = throat area
$a$ = sonic velocity
$b$ = $\dot{r}/pn$
$c_p$ = specific heat at constant pressure
$\dot{m}$ = mass flow rate
$n$ = burning rate pressure exponent
$p$ = pressure
$R$ = gas constant
$r$ = radius or radial coordinate
$\dot{r}$ = propellant burning rate
$T$ = temperature
$t$ = time
$U$ = radial velocity
$V$ = tangential velocity
$W$ = axial velocity
$z$ = axial coordinate
$\gamma$ = ratio of specific heats
$\epsilon$ = nozzle contraction ratio
$\rho$ = density
$\Psi$ = stream function
$\omega$ = angular velocity

### *Subscripts*

$b$ = conditions at burning surface
$c$ = conditions in the chamber
$CL$ = centerline conditions
$o$ = stagnation conditions
$p$ = propellant property
$w$ = conditions at chamber or port wall

Received December 2, 1968; revision received April 24, 1969. The work presented in this paper was supported by the Propulsion Laboratory, U.S. Army Missile Command, Redstone Arsenal, Ala., under Contract DA-01-021-AMC-15257(Z). The continuing interest and assistance of W. Guthrie, the technical monitor for the contract, were of great benefit and are gratefully acknowledged. The authors are indebted to S. Enselman for preparing the illustrations.

* Research Assistant in Mechanical Engineering; now Captain U.S. Army Ord. Corps, assigned to the Jet Propulsion Laboratory, Pasadena, Calif. Member AIAA.

† Research Assistant in Mechanical Engineering; now with the Boeing Company, Seattle, Wash. Member AIAA.

‡ Associate Professor of Mechanical Engineering. Member AIAA.

## Introduction

EARLY in the development of spinning solid-propellant rocket motors, it was observed that the performance of these motors differed significantly from the performance of the same motors under static conditions. The performance of spinning solid-propellant rocket motors is usually characterized by a shorter burning time and pressure-time and thrust-time traces that differ significantly from their static values.

Considerable effort[1] has been devoted to the study of the effects of rotation, known as "spin effects," on the performance of solid-propellant rocket motors. These spin effects can be separated into two basic categories, namely, the effects of acceleration forces on the combustion process, and the effects of the rotating flow on the chamber and nozzle flowfields. The present investigation was concerned with the gasdynamic effects due to the vortex-nozzle interaction.

Published studies of rotating flows in nozzles have been limited primarily to two types of tangential velocity distributions: the free or irrotational vortex, and the forced or solid-body vortex. The free vortex can be characterized by a velocity potential function from which the property distributions at the throat plane can be obtained. Binnie[2] and Mager[3] employed this technique to show that the effective area of a nozzle throat is reduced by the spinning gases of a free vortex. This reduction of effective throat area causes the mass flow rate to decrease if the chamber pressure is maintained constant. This decrease in mass flow rate is attributed to the decrease in the gas density at the throat, where the tangential velocity is a maximum, and to the appearance of a void region on the centerline, through which no mass flows.

Forced vortex flows in a nozzle, which are similar to the flow in an end-burning solid-propellant rocket motor, have been studied by Bastress,[4] Manda,[5] and King.[6] These investigators assumed that a forced vortex was maintained throughout the nozzle and that the strength of the vortex increased as the flow area decreased. Each of these investigators assumed a different choking criterion at the nozzle throat. The assumption that a forced vortex was maintained throughout the nozzle overspecified the problem in each case, as was pointed out by King.

Experimental investigations by Massier[7–10] of swirling flows in nozzles have been conducted at low swirl intensity. These investigations have shown the existence of backflow regions and small changes in the mass flow through the nozzle. More recently, Guthrie[11] has compiled the results of a large number of firings of spinning solid-propellant rocket motors. These results illustrate the effects of spin rate, contraction ratio, and propellant formulation on the chamber pressure of spinning solid-propellant rocket motors.

The present investigation was undertaken to develop an analytical technique for predicting the gasdynamic behavior in nozzles of rotating flows having arbitrary tangential velocity profiles and to investigate experimentally the validity of the theory with a cold-flow spinning rocket motor employing air as the flowing fluid. The development of the theoretical model, the experimental apparatus, and the results obtained with both are presented in the following discussion.

## Analytical Investigation

The purpose of the analytical investigation of rotating flows in rocket motors presented here was to develop a technique for predicting the operating conditions of a solid-propellant rocket motor for a given rate of rotation and nozzle throat size. For design purposes, it is of interest to determine the throat area required to operate at a given chamber pressure. It is also desirable to develop one analysis which can be applied to all types of propellant grain geometries. Therefore, the form of the tangential velocity distribution in the chamber should not be specified as a free or forced vortex, but should be determined from the solution of the governing equations for each type of grain geometry. It is with these objectives in mind that the following model was developed. The details of this development are presented in Ref. 12.

### Model and Limitations

In the analysis of the flow in a nozzle, it was assumed that the flow properties at the nozzle inlet plane are known. The exact distribution of these properties depends upon the propellant grain configuration and the motor spin rate. The determination of these initial conditions is discussed separately in Ref. 12. A schematic of the physical model under consideration is presented in Fig. 1. The flow expands from the initial plane to the throat plane which has the minimum cross-sectional area for the given initial conditions. The throat size is not known a priori. Therefore, the determination of the radius of the throat and the properties of the flow at the throat plane are then the fundamental objectives of the analysis.

The flow is assumed to be steady, inviscid, and adiabatic, and the gases are considered to be thermally and calorically perfect. It is further assumed that the convergence angle of the nozzle is sufficiently small and the radius of curvature of the throat is sufficiently large, thus allowing radial velocities and their derivatives to ben eglected. Since the flow is axisymmetric, the derivatives of velocity and thermodynamic properties in the tangential direction are equal to zero.

### Governing Equations

Conservation of mass for the present model is expressed by an integral for the total mass flow at any radial plane

$$\dot{m}_c = \int_0^{r_c} d\dot{m} = \int_0^{r_c} 2\pi\rho W r dr = \text{const} \qquad (1)$$

where $\dot{m}_c$ is the total mass flow generated in the chamber. For convenience in the numerical technique which is based on the present analysis, a stream function was defined as

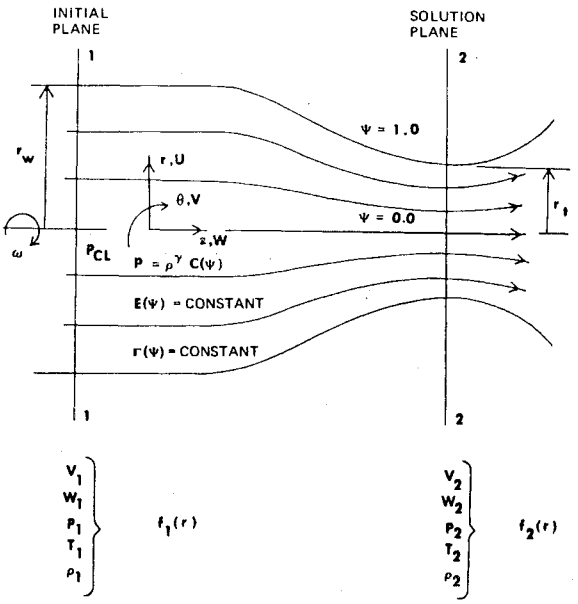


**Fig. 1 Model for the inviscid theory of rotating flow in nozzles.**

follows:

$$\Psi = \int_0^{\dot{m}} \frac{d\dot{m}}{\dot{m}_c} \qquad (2)$$

The stream function varies from zero at the centerline to unity at the nozzle wall. In differential form,

$$d\Psi/dr = 2\pi\rho W r/\dot{m}_c \qquad (3)$$

Under the foregoing restrictions, the entropy and the stagnation enthalpy are constant along each streamline. However, depending upon the initial conditions, these properties may vary from one streamline to the next. Thus, entropy and stagnation enthalpy may be functions of the stream function $\Psi$. Based on this observation, the following equations can be written:

$$E(\Psi) = c_p T_0(\Psi) \text{ constant on streamlines} \qquad (4)$$

$$C(\Psi) = \bar{p}/\bar{\rho}^\gamma \text{ constant on streamlines} \qquad (5)$$

where $\bar{p} = p/p_{\text{ref}}$, $\bar{\rho} = \rho/\rho_{\text{ref}}$, and $p_{\text{ref}}$ and $\rho_{\text{ref}}$ are convenient reference values.

Conservation of momentum for the present model is expressed by the three component Euler equations, neglecting radial velocities and all derivatives in the tangential direction. However, under the assumption of inviscid flow, Bernoulli's equation along a streamline can be used to replace any of the three Euler equations. For the isentropic flow of a thermally and calorically perfect gas, Bernoulli's equation along a streamline and the constancy of stagnation enthalpy along a streamline are equivalent statements. Hence, Bernoulli's equation is not an independent relationship in the present analysis. Thus, only two of the three component Euler equations can be used in the formulation of the present model. The two Euler equations chosen are the tangential and radial momentum equations

$$U\partial V/\partial r + W\partial V/\partial z + UV/r = 0 \qquad (6)$$

$$U\partial U/\partial r + W\partial U/\partial z - V^2/r = -(1/\rho)\partial p/\partial r \qquad (7)$$

The parameter $\Gamma$, which is proportional to the circulation around a stream shell, is defined as follows:

$$\Gamma = Vr \qquad (8)$$

Substituting the definition of $\Gamma$ into Eq. (6) yields

$$U\partial\Gamma/\partial r + V\partial\Gamma/\partial z = D\Gamma/Dt = 0 \quad (9)$$

Therefore, $\Gamma$ is constant along streamlines, and Eq. (9) may be replaced by the following equivalent expression:

$$\Gamma = Vr = \Gamma(\Psi) \text{ constant on streamlines} \quad (10)$$

Substituting the definition of $\Gamma$ into Eq. (7) yields

$$dp/dr = \rho\Gamma(\Psi)^2/r^3 \quad (11)$$

Thus, there are two differential equations (3) and (11) which must be integrated across radial planes and three algebraic equations (4, 5, and 10) which are valid along the streamlines.

Combining Eqs. (4, 5, and 10) and solving for the axial velocity $W$ yields

$$W = \pm\{2c_pT_{\text{ref}}[T_0(\Psi)/T_{\text{ref}} - \bar{p}^{(\gamma-1)/\gamma}C(\Psi)^{1/\gamma}] - \Gamma(\Psi)^2/r^2\}^{1/2} \quad (12)$$

The negative sign denotes a reverse flow; hence, the positive sign is generally employed. $T_{\text{ref}}$ is the temperature corresponding to $p_{\text{ref}}$ and $\rho_{\text{ref}}$.

For convenience in the numerical work, the following dimensionless variables were defined:

$$\bar{E}(\Psi) = T_0(\Psi)/T_{\text{ref}} \quad (13)$$

$$\bar{\Gamma}(\Psi) = \Gamma(\Psi)/V_cr_c = \Gamma(\Psi)/\Gamma_{\text{ref}} \quad (14)$$

$$\bar{r} = r/r_c \quad (15)$$

The final form of the governing differential equations (3) and (11) was obtained by substituting Eq. (12) into (3) and then introducing the definition of the dimensionless parameters into both equations;

$$d\bar{p}/d\bar{r} = [\bar{p}/C(\Psi)]^{1/\gamma}[\bar{\Gamma}(\Psi)^2/\bar{r}^3][\Gamma_{\text{ref}}^2/RT_{\text{ref}}r_c^2] \quad (16)$$

$$d\Psi/d\bar{r} = \pm[2\pi r_c^2\rho_{\text{ref}}(2c_pT_{\text{ref}})^{1/2}/\dot{m}_c][\bar{p}/C(\Psi)]^{1/\gamma}\{\bar{E}(\Psi) - \bar{p}^{(\gamma-1)/\gamma}C(\Psi)^{1/\gamma} - [\Gamma_{\text{ref}}^2/2c_pT_{\text{ref}}r_c^2][\bar{\Gamma}(\Psi)^2/\bar{r}^2]\}^{1/2}\bar{r} \quad (17)$$

The differential equations (16) and (17) have two dependent variables $\bar{p}$ and $\Psi$ which are functions of the single independent variable $\bar{r}$. The integration of these equations at the plane of minimum radius gives the desired information to determine the distribution of all the flow properties at the throat and the radius of the choking plane.

It remains to describe the method of finding the throat plane, where the wall radius is a minimum. This is most readily accomplished by examining the following boundary conditions which are applicable at any downstream plane:

$$\bar{r} = 0, \Psi = 0.0, \bar{p} = \bar{p}_{CL}$$
$$\bar{r} = \bar{r}_w, \Psi = 1.0, \bar{p} = \bar{p}_w \quad (18)$$

Unfortunately, the centerline pressure at the throat plane is not known a priori. Therefore, an iterative procedure is employed to find the centerline pressure such that the wall radius obtained after integrating the governing equations from $\Psi = 0.0$ to $\Psi = 1.0$ is a minimum. It is also possible to formulate the problem of obtaining the minimum wall radius for a flow of this type in terms of classical calculus of variations theory. However, this results in no savings of computational effort.

It was not possible to satisfy the governing equations for all centerline pressures assuming a positive axial velocity. A negative axial velocity indicates a region of reverse flow which the present theory does not adequately describe. However, it was possible to avoid these regions by initiating the numerical solution at some distance away from the centerline. The region between this radius and the centerline was assumed to contain a recirculating flow which did not contribute to the mass, momentum, or energy of the main flow. The size of this reverse flow region was found to decrease as the centerline static pressure decreased and disappeared completely before the throat plane was reached, in all cases investigated numerically. These conclusions have been verified experimentally by Lewellen et al.[13]

### Initial Conditions

In the development of the analytical model for the nozzle flow, it was assumed that the chamber flowfield was known. Knowledge of the chamber flow properties is necessary because the solution of the governing equations at the throat depends upon the initial distribution of the stagnation enthalpy, the angular momentum, the axial velocity, and the thermodynamic properties at the nozzle inlet. Some of the factors which influence the nozzle inlet properties are the propellant composition, the propellant grain geometry, and the rate of rotation of the motor. If this information and a chamber pressure are specified, the flow at the nozzle inlet can be derived for simple grain shapes. Reference 12 presents detailed derivations of the initial conditions for end-burning and internal-burning, cylindrical port grains.

### Viscous Corrections to the Inviscid Theory

The effect of viscosity and turbulence is to reduce and redistribute the angular momentum of the flow. Therefore, the solution of the equations of motion for inviscid flow should be considered as an upper bound on the effects due to rotation. To estimate the effects of viscosity and turbulence, an approximate solution for the tangential momentum equation was obtained by employing finite-difference techniques. The effects of turbulent momentum transport were included by employing an empirical correlation for a "virtual" viscosity. This analysis was used to correct the inviscid theory by accounting for the decrease in $\Gamma(\Psi)$ experienced by the gases as they flow through the nozzle. The correction for the decrease in $\Gamma(\Psi)$ was implemented in the inviscid model by setting the values of $\Gamma(\Psi)$ at the nozzle inlet equal to those predicted at the throat by the viscous flow model. The parameters $\bar{E}(\Psi)$ and $C(\Psi)$ were recalculated for the new values of $\Gamma(\Psi)$.

Thus, the initial conditions were altered so that the angular momentum, stagnation enthalpy, and entropy at the initial plane reflected the expected changes due to viscous dissipation. It was found that this correction improved the correlation between the analytical prediction and the experimental data. The details of this analysis are presented in Ref. 13.

### Numerical Techniques

The fundamental numerical problem was to obtain the centerline pressure for which the wall radius was minimized. To accomplish this, it was necessary to integrate Eqs. (16) and (17) for various centerline pressures. The integration was carried out using a fourth-order Runge-Kutta integration scheme. The integration was initiated at $\Psi = 0.0$ and was continued until $\Psi = 1.0$. The centerline pressure was determined by increasing in finite increments from a value lower than that expected until the minimum wall radius was passed, then reducing the increment size and repeating the procedure until the desired degree of convergence was obtained. In this way, the throat size for a given set of initial conditions was determined. To find the chamber conditions for a given throat size and rate of rotation, it was necessary to repeat this operation for different chamber conditions until the desired throat size was obtained. A more detailed explanation of the numerical methods and problems of solution are presented in Ref. 12.

## Experimental Investigation

An experimental investigation of the effect of spin on the interior ballistics of spinning solid-propellant rocket motors

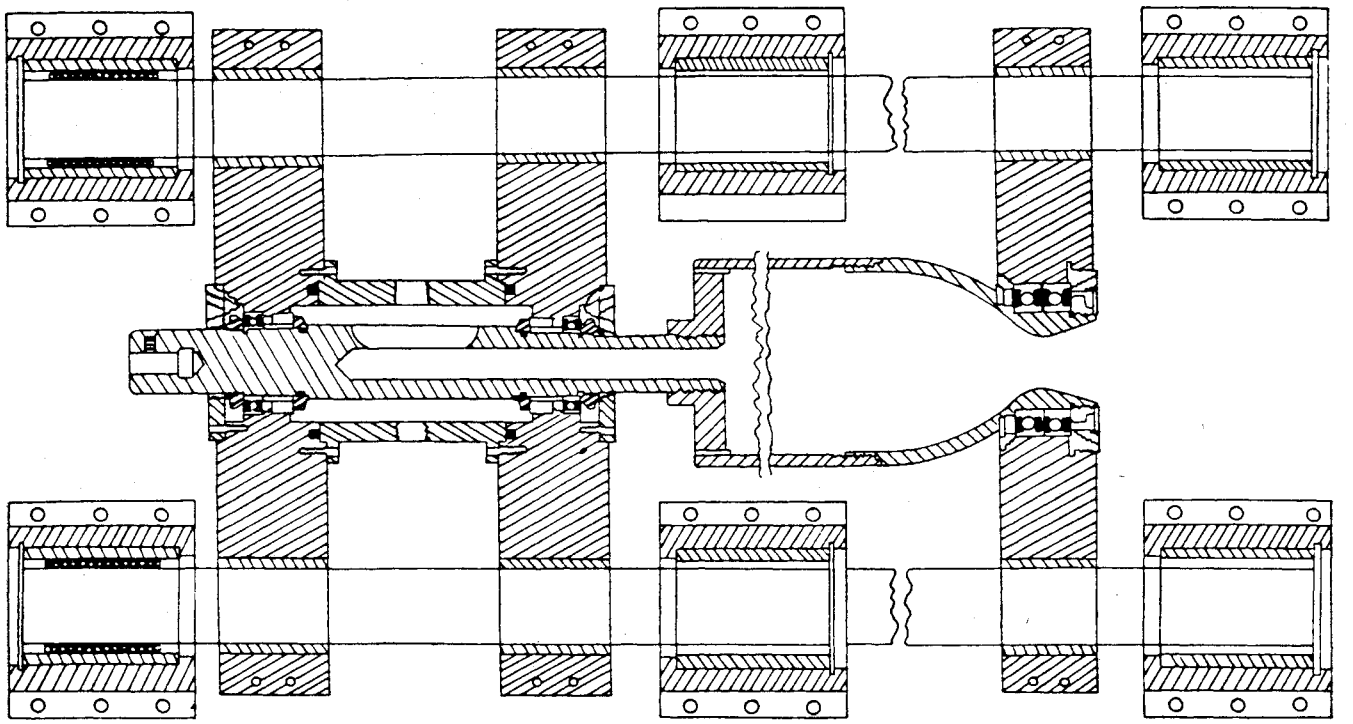

**Fig. 2 Schematic of spinning rocket motor system.**

could be based on any one of several different approaches, for example, a study of the performance of actual spinning solid-propellant rocket motors or a cold-flow study using air as the flowing medium. The abundance of literature describing test firings of spinning rocket motors and the adverse conditions for probing which exist in an actual rocket motor indicated that a cold-flow experimental program would be the most useful. This type of experimental study allowed simulation of both end-burning and internal-burning cylindrical grains, permitted easily controlled variations of mass flow rate, rotational speed, and contraction ratio, and provided a flowfield which was more compatible to probing.

The current investigation was concerned with the extent to which the mass flow rate through a choked nozzle was influenced by the presence of a spinning flowfield. The change in the mass flow rate due to the vortex-nozzle interaction will henceforth be referred to as vortex choking.

The experimental results were used to provide a comparison for the existing theoretical studies of Norton et al.,[12] Mager,[3] Bastress,[4] and Manda.[5] The variables investigated in this study were the motor spin rate, the nozzle contraction ratio or port to throat area ratio, the mass flow rate (i.e., chamber pressure), the propellant grain configuration (i.e., the type of vortex generated), the nozzle configuration, and the location of propellant surface with respect to the nozzle throat. A more complete description of this study is presented in Ref. 14.

### Description of Experimental Apparatus

A schematic drawing of the general arrangement of the cold-flow spinning rocket motor apparatus is presented in Fig. 2. The spinning rocket motor was supported horizontally on four high-speed ball bearings, two of which were mounted in tandem at the motor nozzle. Two additional bearings supported the driving shaft, which in turn was connected to the head end of the motor chamber. The motor casing was approximately 18 in. long with a 6-in. i.d. A set of five nozzles provided contraction ratios of 7.5 to 215.0 for the simulated end-burning grain. The same nozzles, when used with the simulated internal-burning grain which had an i.d. of 2.5 in., yielded port to throat area ratios from 1.56 to 44.4. Air was fed to the motor through slots in the hollow drive shaft.

The type of vortex created inside the motor, whether forced or free, was determined by the manner in which the tangential velocity was imparted to the gas. In this study, a rotational or forced vortex was created by a simulated end-burning propellant grain which, when rotated, yielded a tangential velocity profile of the form $V = r\omega$. This grain consisted of a 1-in.-thick aluminum disk containing 696 holes each $\frac{1}{8}$ in. in diameter, drilled symmetrically about the disk center. This disk was held in place inside the motor by a system of sleeves which allowed the location of the grain to be varied along the axis of the motor. An irrotational or free vortex, characterized by a tangential velocity profile of the form $V = k/r$, was created by a simulated internal-burning cylindrical propellant grain. This grain consisted of a 13-in.-long tube with a 4-in. o.d. and a 2.5-in. i.d. This tube contained 588 holes each $\frac{1}{4}$ in. in diameter, drilled radially. Both of the simulated grains were retained in position inside the motor chamber by the nozzle.

The bearing housings supporting the entire rotating assembly were rigidly attached to two 2.5-in.-diam rods; these rods in turn were supported in linear ball bushings. The spinning cold-flow rocket motor was driven by a Barbour Stockwell 8-in. air turbine connected to the drive shaft of the spinning rocket motor by a quill shaft arrangement.

The air used in the cold-flow study was obtained from a system of storage tanks at an initial pressure between 1500 and 2500 psig. The air was dried and filtered, and the pressure was reduced through a pressure-regulating valve before entering the cold-flow apparatus. An American Society of Mechanical Engineers orifice and the associated instrumentation were employed to measure the mass flow rate.

Initial studies of the vortex choking phenomena made with the simulated end-burning grain did not yield as large a reduction in mass flow rate as was expected. Further investigation of the flowfield indicated that, as a result of the higher pressure near the wall due to the presence of the radial pressure gradient across the grain face, the flow tended to concentrate near the axis of the grain instead of flowing uniformly through the entire face of the grain. The installation of a piece of sintered stainless plate at the back face of the simu-

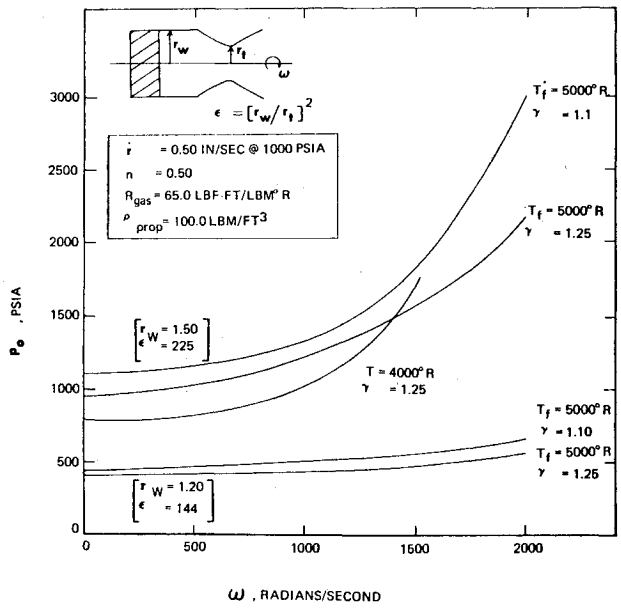


**Fig. 3 Chamber pressure as a function of the rate of rotation for end-burning motors with various propellant properties.**

lated end-burning grain created an axial pressure drop of sufficient magnitude so that the radial pressure gradient was negligible compared to the axial pressure gradient. This resulted in a reasonably uniform mass flow rate per unit area through the simulated end-burning grain.

A typical study involved establishing the desired conditions of contraction ratio, nozzle configuration, grain design and location, and the nonrotating mass flow rate. Rotation of the motor was initiated and the spin rate was increased slowly up to the desired maximum speed while the mass flow rate was monitored as a function of the rotational speed. Similar measurements were made as the rotational speed was decreased. The results of these investigations are presented in the following section.

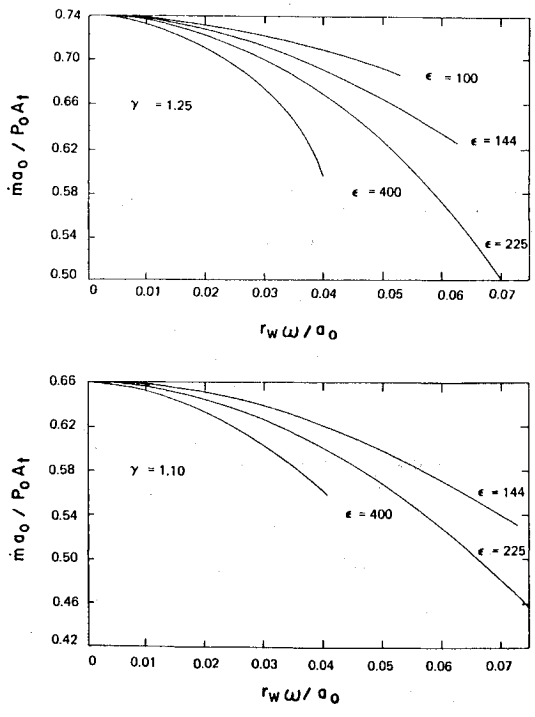


**Fig. 4 Effect of contraction ratio on the performance of end-burning motors as a function of rate of rotation.**

## Results

In this section, the results of the analytical and experimental investigations are presented. Some computations for typical conditions representing solid-propellant rocket motors and the experimental and analytical results for the cold-flow studies are discussed.

### Analytical Results for Solid-Propellant Motors

Figure 3 presents some typical results for the variation of the centerline chamber pressure with the speed of rotation for end-burning motors. By comparing the shapes of the curves for contraction ratios $\epsilon_c$ of 144 and 225, it can be seen that increasing the contraction ratio increases the sensitivity of the chamber pressure to rotation. In addition, decreasing the flame temperature $T_f$ and specific heat ratio increases the sensitivity to rotation. These effects can be explained qualitatively in the following manner. Decreasing the specific heat ratio and the flame temperature tends to decrease the sonic velocity of the gas; hence the axial velocity in the throat region is reduced. Increasing contraction ratio tends to increase the tangential velocity at the throat due to the conservation of angular momentum. Thus, the ratio of the tangential velocity to the axial velocity becomes larger at the throat for increasing contraction ratio and decreasing specific heat and flame temperature of the propellant gases. As this velocity ratio at the throat increases, the integrated mass flow at the throat decreases, resulting in the increased pressures shown in Fig. 3. An increase in molecular weight was found to affect the chamber pressure in the same manner as a decrease in flame temperature or specific heat ratio.

The results of an extensive parametric study of the effect of spin on end-burning motors are presented in Fig. 4. The mass flow parameter $\dot{m}a_0/p_0A_t$, which for one-dimensional flow is a function of the specific heat ratio of the flowing gas, is plotted as the ordinate. The swirl parameter $r\omega/a_0$, which is the tangential velocity at the wall of the chamber nondimensionalized with respect to the stagnation acoustic speed, is plotted as the abscissa. Each curve in these figures represents a particular contraction ratio $\epsilon$. Each set of curves corresponds to a particular specific heat ratio $\gamma$. The results presented in these figures were obtained for a range of flame temperatures (2500–5000°R), molecular weights (24.0–34.0), burning rates, (0.2–0.5 in.-sec), motor diameters (2.0–4.0 in.), and specific heat ratios (1.1–1.3).

Employing Fig. 4, the chamber pressure for a particular contraction ratio can be determined at any rate of rotation

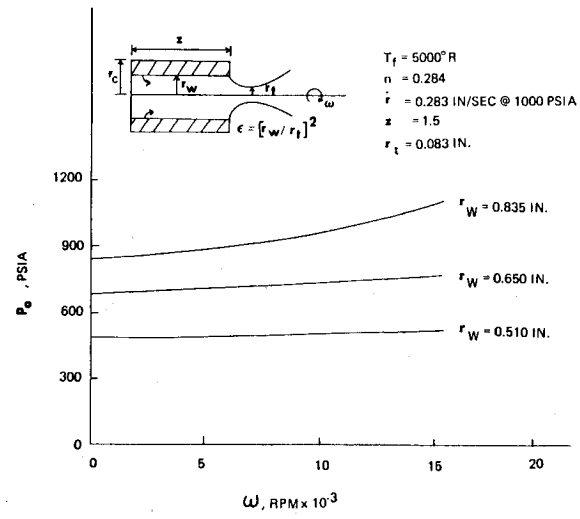


**Fig. 5 Chamber pressure as a function of rate of rotation and propellant radius for a typical internal-burning motor.**

for a particular rocket motor. This is accomplished by expressing the mass flow rate as follows:

$$\dot{m}2 = \pi b \rho_p \int_0^{r_c} p^n r dr \tag{19}$$

Because the chamber pressure does not vary greatly across the propellant surface, Eq. (19) can be integrated to obtain the following approximate relationship:

$$\dot{m}a_0/A_t p_0 = b\rho_p p^n a_0 A_b = b\rho_p p^{n-1}(A_b/A_t) \tag{20}$$

For a given contraction ratio $(A_b/A_t)$ and stagnation acoustic speed, the chamber pressure at which the motor operates can thus be found from Eq. (20) and Fig. 4.

For internal-burning grains, the propellant surface area changes as the surface recedes. This causes changes in chamber pressure as the propellant burns. For a rotating rocket motor, the chamber pressure varies with the rate of rotation as well. Figure 5 presents the head-end pressure at the propellant burning surface as a function of the rate of rotation for three propellant surface radii for typical motor operating conditions. When the radius is small, the pressure remains relatively constant with increasing speed of rotation. As the surface recedes and the propellant radius increases, the angular momentum in the flow also increases. This causes the chamber pressure to become more sensitive to the rate of rotation. The increase in pressure due to increases in the surface area combined with the vortex-nozzle interaction can result in large chamber pressures prior to burnout.

The progressivity of the grain can be eliminated by employing end-burning faces on the internal-burning grain. Figure 6 presents the chamber pressure variation for a typical motor of this type. In the case illustrated, the surface area of the propellant is actually decreasing with time. Therefore, the chamber pressure at zero rotation decreases as the propellant burns. At high speeds of rotation, the chamber pressure tends to increase with increasing radius of the propellant surface.

### Experimental Cold-Flow Results

The results presented in this section were obtained from the cold-flow studies described previously. The data are presented in terms of the mass flow rate parameter $\dot{m}a_0/p_0A_t$ vs the swirl parameter $r_w\omega/a_0$ for several contraction ratios or

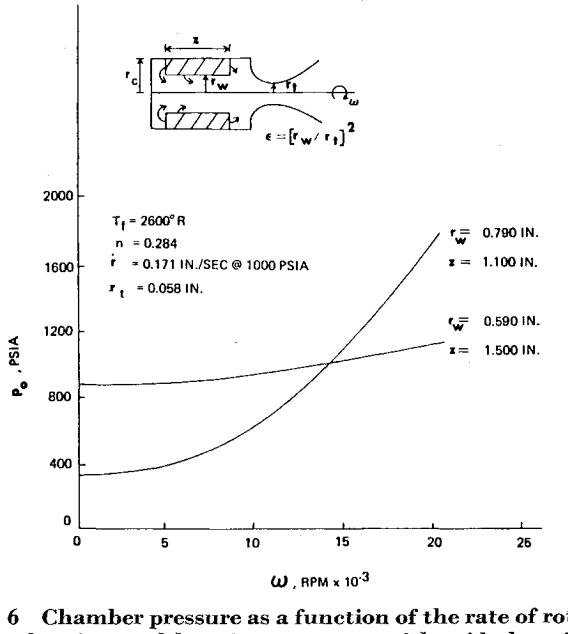


**Fig. 6 Chamber pressure as a function of the rate of rotation for internal-burning motors with side-burning faces.**

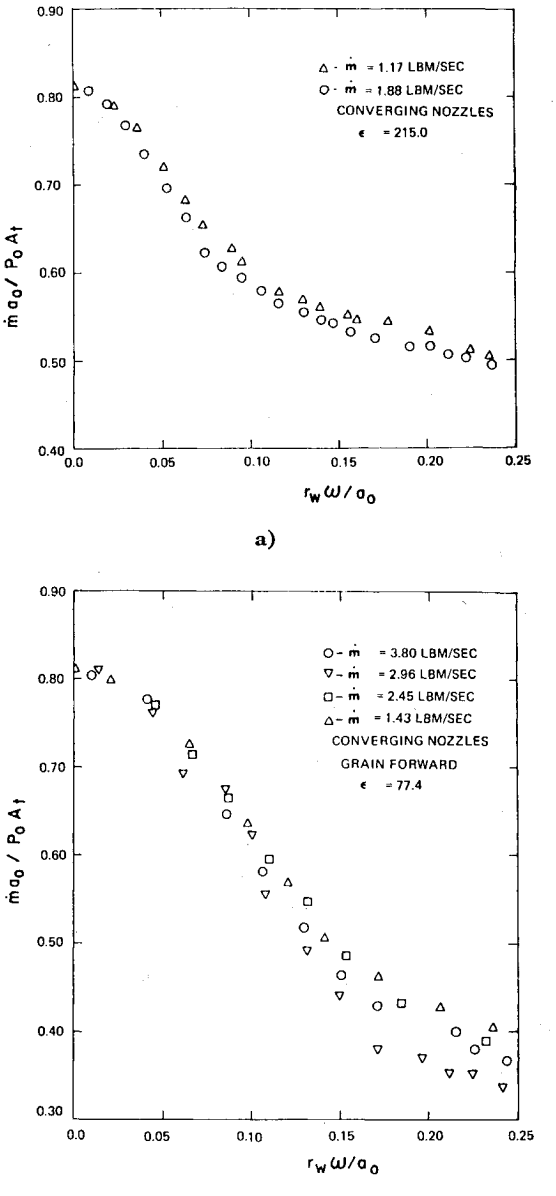


**Fig. 7 Effect of mass flow rate on forced vortex choking.**

port to throat area ratios $(r_w/r_t)^2$. The radius $r_w$ is defined as the motor chamber radius for the end-burning grain and is defined as the port radius for the internal-burning cylindrical grain. The pressure $p_0$ is a representative chamber pressure obtained by subtracting from the measured orifice pressure the measured pressure drop from the orifice to the spinning motor.

Figures 7a and 7b illustrate the effects of different mass flow rates on vortex choking with the same motor geometry but different contraction ratios. These data show a mass flow rate reduction due to the tangential velocity component, but little, if any, effect due to the magnitude of the mass flow rate itself. This is illustrated by the close grouping of the points for the same rotational speed on each of the curves. Thus, since the mass flow rate appears to have a negligible influence on vortex choking, comparisons of results need not be made at identical mass flow rate or chamber pressure conditions.

The influence of contraction ratio on vortex choking for a forced vortex is presented in Fig. 8. These data indicate that the larger the contraction ratio, the more significant is the mass flow rate reduction because of vortex choking. For

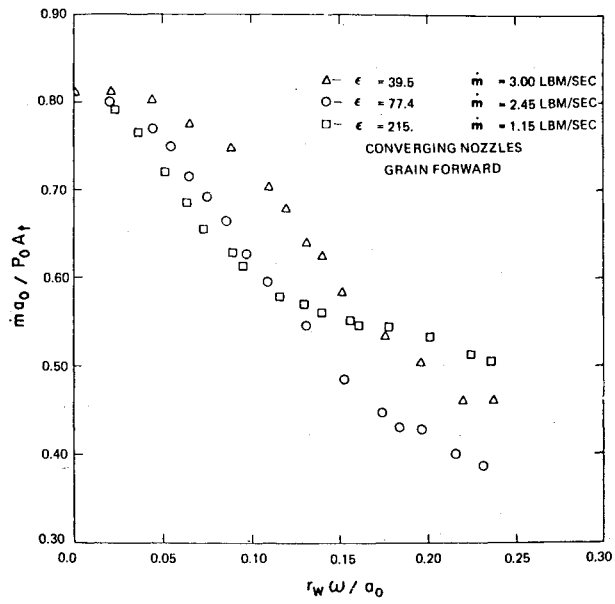


**Fig. 8 Effect of contraction ratio on forced vortex choking.**

the contraction ratio of 215, the mass flow parameter decreases continuously as the swirl parameter increases up to a value of approximately 0.12. However, an increase in the swirl parameter beyond 0.12 produces less of a change in the mass flow parameter for any further increase in the swirl parameter. This effect was not observed in the studies with contraction ratios of 39.5 and 77.4.

Similar results showing a decrease in the mass flow parameter for increasing values of the swirl parameter were obtained for the simulated internal-burning grain. The $\frac{5}{8}$- and $\frac{3}{8}$-in.-diam nozzles used with the 2.5-in.-i.d. grain yielded port to throat area ratios of 16.0 and 44.4, respectively. The data for these tests are shown in Fig. 9 for the two different port to throat area ratios. These data indicate that an increase in the port to throat area ratio increases the vortex choking effect of a free vortex for a constant value of the swirl parameter. However, the results for the free vortex studies did not show a tendency for the mass flow parameter to approach a region of less sensitivity to swirl at large values of the swirl parameter as was the case for the forced vortex flow with a large contraction ratio.

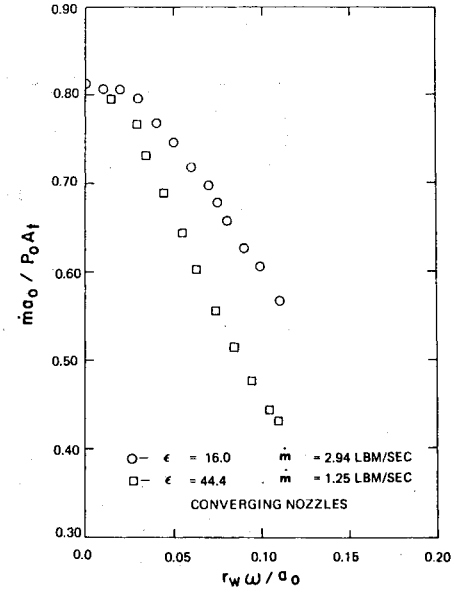


**Fig. 9 Effect of contraction ratio on free vortex choking.**

To investigate the dependence of vortex choking on the magnitude of the mass flow rate for internal-burning grains, data for each nozzle using the simulated internal-burning grain were obtained at several mass flow rates. These data are presented in Figs. 10a and 10b. Here, as in Figs. 7a and 7b for the simulated end-burning grain, the data fall on one relatively smooth curve, thus showing an insignificant effect of the mass flow rate on vortex choking.

Similar studies conducted with free and forced vortices but using converging-diverging nozzles yielded data identical to that obtained with the converging nozzles. Thus, as would be expected, the contraction ratio and not the nozzle contour downstream of the throat is the dominant parameter in vortex choking. Other studies indicated that the location of the simulated end-burning grain in the chamber had a negligible influence on vortex choking.

### Discussion of Results and Comparison

One of the major factors influencing the mass flow rate reduction in the cold-flow experiments due to the interaction of a swirling flow with a nozzle is the type of swirl or vortex initially generated. Typical results of vortex choking for a

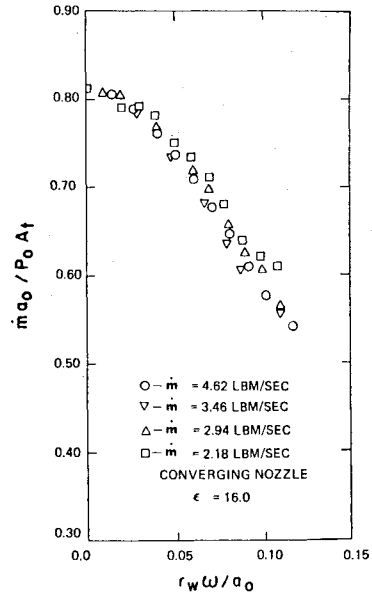


a)

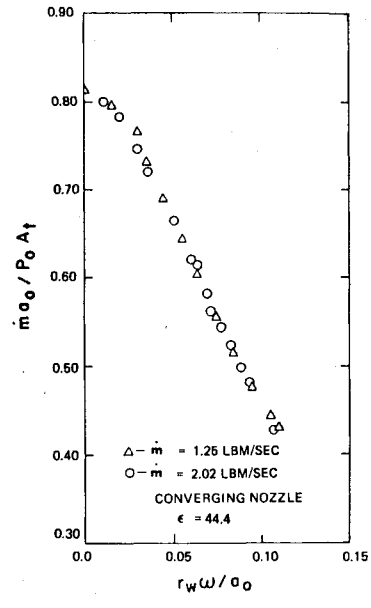


b)

**Fig. 10 Effect of mass flow rate on free vortex choking.**

forced and a free type vortex were presented in Figs. 8 and 9, respectively. It should be pointed out that the results presented on these two figures are not for the same nozzle throat diameter. The abscissa ($r_w\omega/a_0$) specifies the vortex strength of each type of vortex. This parameter is proportional to the maximum tangential velocity generated at the face of the vortex generating surface (i.e., the simulated grain).

The results of the experimental studies of vortex choking when the initial flow was a forced vortex were presented in Fig. 8 for nozzle contraction ratios of 39.5, 77.4, and 215. As can be seen from these data, the magnitude of the mass flow rate reduction is strongly influenced by the strength of the vortex. All three contraction ratios show a continuous decrease in the flow rate parameter as the swirl parameter increases from zero. This trend is continuous for contraction ratios of 39.5 and 77.4 up to the largest values of the swirl parameter investigated.

Comparisons of the analytical inviscid and viscous predictions for air flowing at a total temperature of 520°R in a forced vortex pattern, with experimental measurements

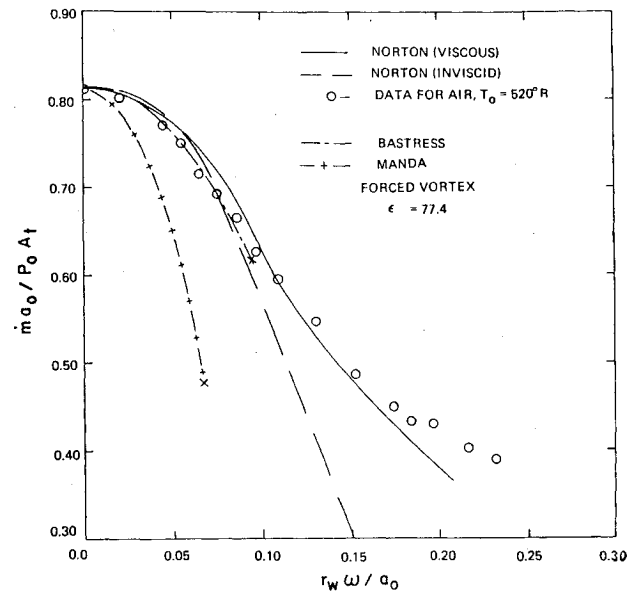


a)

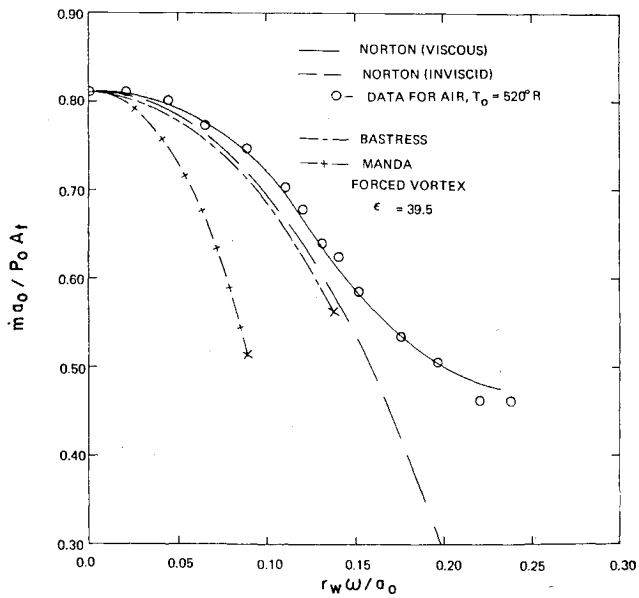


b)

**Fig. 11 Comparison of analytical and experimental results, forced vortex.**

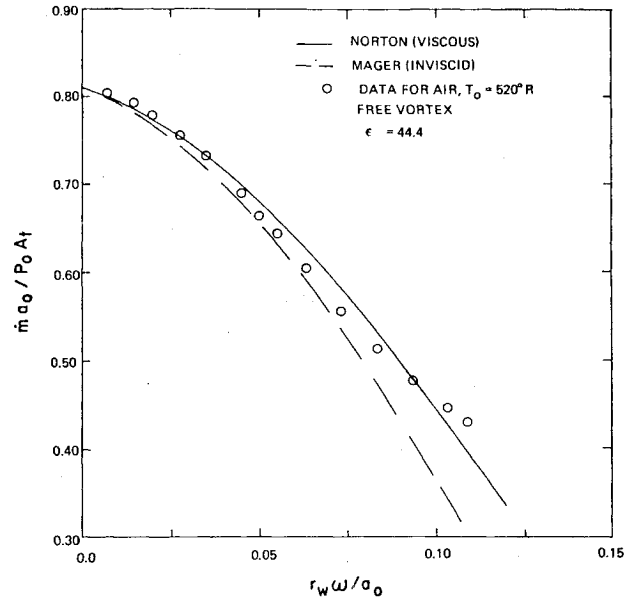


**Fig. 12 Comparison of analytical and experimental results, free vortex.**

made at similar conditions, for contraction ratios of 77.4 and 39.5 are shown in Figs. 11a and 11b, respectively. These comparisons indicate that the viscous analysis predicts quite accurately the mass flow rate reduction resulting from the vortex-nozzle interaction. The inviscid solution overpredicts the vortex choking, as would be expected.

The experimental studies of a free vortex interaction with a nozzle employed a simulated internal-burning solid propellant grain to impart a tangential velocity to the air. The results of free vortex choking studies are presented in Fig. 9 for port to throat area ratios of 16.0 and 44.4. As in the studies of the forced vortex, the mass flow rate parameter $\dot{m}a_0/p_0A_t$ decreased as the vortex strength $r_w\omega/a_0$ increased.

It is noteworthy that the vortex choking trend shows no tendency to become less sensitive to swirl over the full range of the swirl parameter investigated for both port to throat area ratios. Figures 10a and 10b presented data for a port to throat area ratio of 16.0 for four different mass flow rates and for a port to throat area ratio of 44.4 for two different mass flow rates. These data indicate, as did the studies of forced vortex flows, that the mass flow rate (i.e., chamber pressure) has, at most, a secondary effect on the mass flow rate reduction caused by the interaction of a free vortex and a nozzle.

The data obtained for the free vortex interaction with a converging nozzle at a port to throat area ratio of 44.4 are presented in Fig. 12, along with predictions from Mager's[3] inviscid theory and the viscous theory due to Norton et al.[12] The analytical solutions and the experimental results are both for air having a total temperature of 520°R and identical port to throat area ratios. Both of the analytical solutions agree closely with the measured data. The viscous solution appears to be slightly more realistic at the larger values of the swirl parameter where the stronger vortex would be more susceptible to viscous dissipation because of larger velocity gradients.

## Conclusions

The results of the present investigation of swirling flow in nozzles justify the following conclusions:

1) The presence of a swirl component in a flow through a nozzle will produce a reduction in the mass flow rate through the nozzle.

2) The degree to which the mass flow rate through a nozzle is influenced by the swirl component is strongly dependent

on the extent to which the flow area is reduced (i.e., the contraction ratio), the relative strength of the vortex, and whether the initial flow has the characteristics of a free or forced vortex.

3) For a given set of propellant properties (i.e., specific heat ratio, molecular weight, and stagnation temperature), the mass flow rate or chamber pressure has little, if any, effect on the degree to which vortex choking occurs.

4) The vortex choking caused by swirling flow in a nozzle is not significantly influenced by the type of nozzle contour (i.e., converging or converging-diverging).

5) The location of the forced vortex generating surface in a spinning chamber upstream of a nozzle has a negligible influence on the vortex-nozzle interaction.

6) For forced vortex flows, the swirl parameter reaches a value beyond which the mass flow rate is less sensitive to swirl. This limit of vortex choking is apparent in nozzles with large contraction ratios where a large swirl component is present.

7) The analytical model due to Norton et al.[12] accurately predicts the vortex choking phenomenon in a nozzle for both forced and free vortex flows. For flows with a large swirl component, the viscous model appears more accurate than the inviscid model.

## References

[1] Norton, D. J., Farquhar, B. W., and Hoffman, J. D., "Analytical Studies of the Interior Ballistics of Spin Stabilized Rocket Motors—A Literature Survey," Rept. TM-67-1, Jan. 1967, Jet Propulsion Center, Purdue Univ.

[2] Binnie, A. M., "The Passage of a Perfect Fluid Through a Critical Cross-Section or 'Throat'," *Proceedings of the Royal Society (London), Series A*, Vol. 197, 1949, pp. 545–555.

[3] Mager, A., "Approximate Solution of Isentropic Swirling Flow Through a Nozzle," *ARS Journal*, Vol. 31, No. 8, Aug. 1961, pp. 1140–1148.

[4] Bastress, E. K., "Interior Ballistics of Spinning Solid Propellant Rockets," *Journal of Spacecraft and Rockets*, Vol. 2, No. 3, May-June 1965, pp. 455–457.

[5] Manda, L., "Spin Effects on Rocket Nozzle Performance," *Journal of Spacecraft and Rockets*, Vol. 3, No. 11, Nov. 1966, pp. 1695–1696.

[6] King, M. K., "Spin Effects on Rocket Nozzle Performance," *Journal of Spacecraft and Rockets*, Vol. 3, No. 12, Dec. 1966, pp. 1812–1813.

[7] Massier, P. F., "Axisymmetric Steady Flow of a Swirling Compressible Fluid Through a Convergent-Divergent Nozzle without External Heat Transfer," *Jet Propulsion Laboratory Space Programs Summary No. 37-33*, Vol. IV, June 1965, pp. 133–141.

[8] Massier, P. F., "Swirling Flow of Argon Through an Axisymmetric Convergent-Divergent Nozzle," *Jet Propulsion Laboratory Space Programs Summary No. 37-34*, Vol. IV, Aug. 1965, pp. 149–163.

[9] Massier, P. F., "Thrust Comparisons for Swirling and Non-Swirling Flows of Argon Through a Convergent-Divergent Nozzle as Determined from Wall Pressure Measurements," *Jet Propulsion Laboratory Space Programs Summary No. 37-35*, Vol. IV, Oct. 1965, pp. 161–165.

[10] Massier, P. F., "Static Pressure Drop along the Wall of a Constant Diameter Duct Which Contains a Decaying Swirling Flow of Argon," *Jet Propulsion Laboratory Space Programs Summary No. 37-36*, Vol. IV, Dec. 1965, pp. 117–126.

[11] Guthrie, W. D., unpublished data, July 1967, obtained at the Propulsion Laboratory, Redstone Arsenal, Ala.

[12] Norton, D. J., Farquhar, B. W., and Hoffman, J. D., "An Analytical Investigation of the Fluid Mechanics of Rotating Flows in Rocket Motors," Rept. TM-67-7, Oct. 1967, Jet Propulsion Center, Purdue Univ.

[13] Lewellen, W. S., Burns, W. J., and Strickland, H. J., "Transonic Swirling Flow," AIAA Paper 68-693, Los Angeles, Calif., 1968; also *AIAA Journal*, Vol. 7, No. 7, July 1969, pp. 1290–1297.

[14] Farquhar, B. W., Norton, D. J., and Hoffman, J. D., "An Experimental Investigation of Swirling Flows in Nozzles," Rept. TM-68-1, Jan. 1968, Jet Propulsion Center, Purdue Univ.